

Review

Solid state nuclear track detectors

C. HEPBURN,* A. H. WINDLE

Department of Metallurgy and Materials Science, Pembroke Street, Cambridge, UK

The materials science aspects of the use of both polymeric and inorganic solids as detectors for energetic particles are reviewed. The various models proposed to explain the formation of an etchable track by a penetrating particle are discussed, as is the nature and the geometric consequences of the etching process itself. An account is given of the wide-ranging applications of solid state detectors in science and technology.

1. Introduction

It is possible to trace, within the history of science, events which represent the founding of a new field of interest and then the subsequent growth of this field to the stage where it achieves recognition as a scientific discipline in its own right. The discovery, development and application of solid state nuclear track detectors (SSNTDs) within the last two decades, is in many ways a good example of the birth and growth of a new discipline. Already these detectors are in use in many diverse branches of science from nuclear physics to geology and from space physics to archeology. In 1975, an extensive and definitive text "Nuclear Tracks in Solids" [1] was published, written by Fleischer, Price and Walker who themselves contributed much to the development of the subject. More recently, 1977, a dedicated journal has made its appearance. It is *Nuclear Track Detection* [2] with S. A. Durrani as its editor.

Solid state nuclear track detectors (SSNTDs) are essentially materials that are damaged in such a way by energetic particles, that the particle tracks can be developed by subsequent etching and observed microscopically (Fig. 1).

Young [3] in 1958, made the first observation of microscopic track formations in the surface of a lithium fluoride crystal that had been irradiated with fission fragments and etched in a mixture of hydrofluoric and acetic acids. One year later, Silk and Barnes [4], working apparently

independently of Young, although in the same laboratories at Harwell, observed with the electron microscope damaged regions in mica which marked the paths of heavy charged particles such as those from fission fragments or cosmic rays. In 1962 Price and Walker [5], unaware of Young's paper, found that these tracks could be enlarged by etching the mica and Fleischer extended this to other materials substantiating it as a general phenomenon in dielectric solids.

2. The scope of the effect

2.1. Recording materials

Etchable tracks may be found in almost any type of electrically insulating material, crystalline, glassy or polymeric, which has been exposed to ionizing particles. They have never been seen in metals or other good conductors. Materials of resistivity $> 2 \times 10^5 \Omega\text{m}$ are known to be capable of recording and storing tracks; materials of lower resistivity apparently do not have this capability [6] as demonstrated in Table I.

It is interesting to note that a threshold resistivity for the production of tracks appears to exist in various semiconductors with some forming tracks (V_2O_5 glass) while others form none (Si, Ge) [7]. Tracks have been observed in thin films of MoS_2 , MoTe_2 (α and β phases), WSe_2 , MoSe_2 , WS_2 and WTe_2 but not in LiSe_2 , LaSe_2 , NbSe_2 , LaTe_2 and NbTe_2 [8]. However, no data are available as to the directions of planes of the crystals used in this work. Electrical

* Permanent address: Institute of Polymer Technology, Loughborough University, Loughborough, Leicestershire, UK.

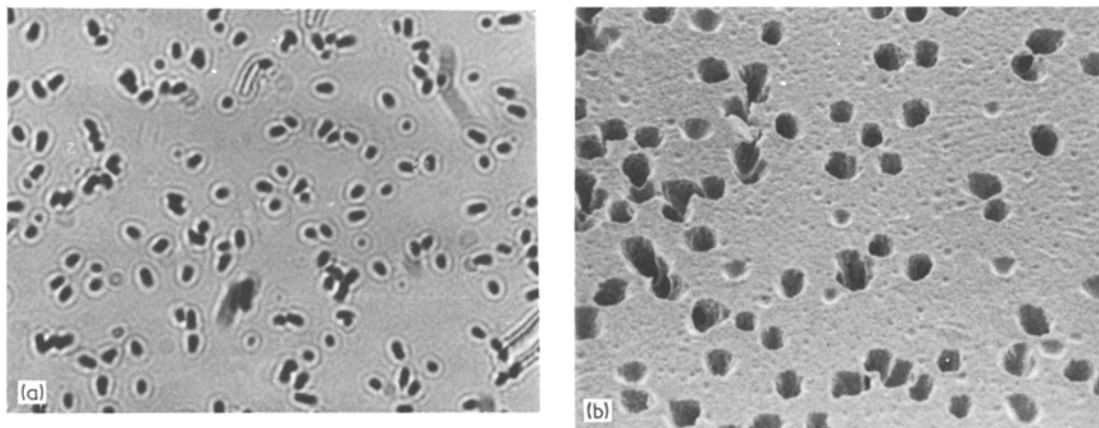


Figure 1 (a) Light micrograph of cellulose nitrate film (LR 115-II, Kodak Pathe, France) irradiated with α particles from ^{241}Am and etched to reveal tracks with 5 M NaOH for 30 min at 55° C, $\times 4050$. (b) Scanning electron micrographs of similar tracks to (a), $\times 6000$.

resistivity may not, of course, be the only parameter to consider in attempts to classify materials and their radiation track responsive properties. It is, however, the most important.

2.2. Threshold sensitivity of a solid

For each dielectric it is possible to establish which radiation particles will register tracks. In polymeric solids the initial effect of ionizing particles on the covalent bonds of the polymer will be to cause bond rupture, and hence along the trajectory of a particle, where a high density of broken bonds will occur, there should be decreased average molecular weight and increased chemical activity. It is necessary to establish which particles will or will not produce etchable tracks; consistent with the hypothesis that for each solid there exists a critical rate of energy loss such that

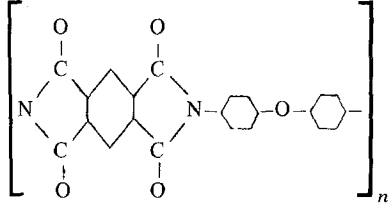
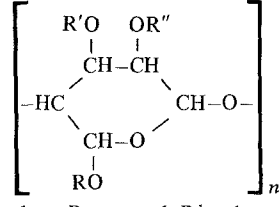
particles losing energy more rapidly than this value produce continuous tracks with unit efficiency, while those depositing appreciably less energy per unit length produce no tracks. Or, described differently, for a given material a given value of Coulomb field must be produced by the positive ions formed in the ionization process before the massive repulsion of these atomic or molecular ions from their lattice sites takes place. Thus, in these materials, an ionization density threshold will exist below which a charged particle will not cause a damage track to be produced. This means that in an etched dielectric material the tracks of very heavy ionizing particles can be made visible while those of electrons, protons and sometimes α -particles, are not seen. This ionization density threshold is a property of the particular dielectric material and can be used to discriminate against low mass particles.

TABLE I Radiation track storing properties and electrical resistivity of materials

Materials	Electrical resistivity (Ωm)
<i>Track forming</i>	
Electrical insulators:	
Silicate minerals	$10^8 - 10^{22}$
Alkali halides	
Insulating glasses	
Polymers	
Poor insulators: MoS_2	$3 \times 10^5 - 25 \times 10^5$
Semiconductors: V_2O_5 , glass	$2 \times 10^5 - 2 \times 10^6$
<i>Non-track forming</i>	
Semiconductors: Si, Ge	$1 \times 10^3 - 2 \times 10^5$
Conductors:	
Metals, Al, Cu, Au, Pt, W, Zn	$10^{-4} - 10^{-2}$

SSNTD materials can be ranked in order of sensitivity. Tables II and III are adapted from the compilation of Fleischer *et al.* [1]. They list a range of different materials and indicate for each the smallest ion that has been observed to form an etchable track, together with the energy of that ion. It is important to note that the data for polymers is often specific to a particular formulation and particles which form tracks in, say, one cellulose nitrate product may have no effect on a nominally similar polymer from a different manufacturer. In addition, registration behaviour can be markedly influenced by etching conditions, for example, temperature, concentration, pre-conditioning by exposure to specific environments

TABLE II Sensitivity order of track detector materials ranked in qualitative classes (adapted from [1])

Material	Composition principal repeating unit(s)	Smallest ionizing ion detected (together with its energy where known)
Polyethylene	$[\text{CH}_2]_n$	
Polystyrene	$[\text{CH}_2 \text{ CH} \text{ C}_6 \text{ H}_5]_n$	Fragments from fission processes
Polyvinylchloride– vinylacetate co-polymer	$\left[\begin{array}{c} \text{CH}_2 - \text{C} \cdot \text{H} \\ \\ \text{Cl} \end{array} \right]_n - \left[\begin{array}{c} \text{CH}_2 \text{ CH} \\ \\ \text{COOCH}_3 \end{array} \right]_m$	42 MeV ^{32}S
Polyvinylchloride– vinylidenechloride co-polymer	$\left[\begin{array}{c} \text{CH}_2 - \text{CH} \\ \\ \text{Cl} \end{array} \right]_n - \left[\text{CH}_2 - \text{C} \text{ Cl}_2 \right]_m$	42 MeV ^{32}S
Polyethylene	$[\text{OC} - \text{C}_6\text{H}_{10} - \text{COO}(\text{CH}_2)_2\text{O}]_n$	
Polyimide		36 MeV ^{16}O
Polyoxymethylene	$[-\text{CH}_2\text{O}-]_n$	28 MeV ^{11}B
Polypropylene	$\left[\begin{array}{c} \text{CH}_2 - \text{CH} \\ \\ \text{CH}_3 \end{array} \right]_n$	1 MeV ^4He
Polyvinylchloride	$\left[\begin{array}{c} \text{CH}_2 - \text{CH} \\ \\ \text{Cl} \end{array} \right]_n$	
Polymethylmethacrylate	$\left[\begin{array}{c} \text{CH}_2 - \text{C} \cdot \text{CH}_3 \\ \\ \text{COOCH}_3 \end{array} \right]_n$	3 MeV ^4He
Cellulose esters	 general structure	3 MeV ^4He
Cellulose acetate butyrate	where R = acetyl, R ¹ = butyrate	
Cellulose triacetate	where R, R ¹ , R ¹¹ = acetyl	
Cellulose nitrate	where R = nitrate	0.55 MeV ^1H

such as ultraviolet light and oxygen. Accordingly some overlap between closely ranked detector materials may occur when these experimental parameters are varied.

Fig. 2 is an alternative way of displaying mass and energy thresholds for various detector–particle combinations. The curves relating primary ionization rate of the detector atoms to particle velocity are calculated for particular detector–particle combinations from a formula originally derived by Bethe in 1930 [9]:

$$J = \frac{C_1 C_2 Z^2}{I_0 \beta^2} \left[\ln \left(\frac{W_{\max}}{I_0} \right) - \beta^2 - \delta + K \right]$$

where J is the primary ionization density, Z the atomic number of the particle, β the relativistic velocity of particle, I_0 the ionization potential of most loosely bound electrons in the detector, $W_{\max} = 2mc^2\beta^2/(1 - \beta^2)$, m the electron mass, c the velocity of light, δ the polarization correction at relativistic velocities, K the recorder material constant, $C_1 = 2\pi ne^4/mc^2$, n the number

TABLE III Inorganic SSNTDs (minerals, crystals, glasses) (adapted from [1])

Material	Composition	Smallest ionizing ion detected and its energy
Diopside	$\text{CaMg}(\text{SiO}_3)_2$	170 MeV ^{56}Fe
Augite	$\text{CaMg}_3\text{Fe}_3\text{Al}_2\text{Si}_4\text{O}_{19}$	170 MeV ^{56}Fe
Hypersthene	$\text{Mg}_{1.5}\text{Fe}_{0.5}\text{Si}_2\text{O}_6$	100 MeV ^{56}Fe
Olivene	MgFeSiO_4	
Orthoclase	KAlSi_3O_8	100 MeV ^{40}Ar
Quartz	SiO_2	100 MeV ^{40}Ar
Soda-lime glass	$23\text{SiO}_2 : 5\text{Na}_2\text{O} : 5\text{CaO} : \text{Al}_2\text{O}_3$	20 MeV ^{20}Ne
Phosphate glass	$10\text{P}_2\text{O}_5 : 1.6\text{BaO} : \text{Ag}_2\text{O} : 2\text{K}_2\text{O} : 2\text{Al}_2\text{O}_3$	
Silica glass	SiO_2	16 MeV ^{40}Ar
Oligoclase	$\text{Na}_4\text{CaAl}_6\text{Si}_{14}\text{O}_{40}$	4 MeV ^{28}Si
Bytownite	$\text{NaCa}_4\text{Al}_9\text{Si}_{11}\text{O}_{40}$	4 MeV ^{28}Si
Phlogopite mica	$\text{KMg}_2\text{Al}_2\text{Si}_3\text{O}_{10}(\text{OH})_2$	
Muscovite mica	$\text{KAl}_3\text{Si}_3\text{O}_{10}(\text{OH})_2$	2 MeV ^{20}Ne
Labradorite	$\text{Na}_2\text{Ca}_3\text{Al}_8\text{Si}_{12}\text{O}_{40}$	
Zircon	ZrSiO_4	
Bronzite	$\text{Mg}_{1.7}\text{Fe}_{0.3}\text{Si}_2\text{O}_6$	
Enstatite	MgSiO_3	
Flint glass	$18\text{SiO}_2 : 4\text{PbO} : 1.5\text{Na}_2\text{O} : \text{K}_2\text{O}$	2–4 MeV ^{20}Ne
Tektite glass (obsidian)	$22\text{SiO}_2 : 2\text{Al}_2\text{O}_3 : \text{FeO}$	

of electrons/cm³ of change e in detector, and C_2 the fraction of electrons in the most loosely bound state.

The velocity is equivalent to energy per nucleon which is essentially the total particle energy divided by its atomic weight. Fig. 2 demonstrates that for a given detector material, particles must exceed a critical mass before they will produce a track. Also, a particle will only register over a certain energy range. A minimum energy is necessary (which is small on the scale of Fig. 2)

and there is an energy cut-off above which the particle is moving too quickly to produce sufficient density of damage. For example ^{16}O particles will record on PET (Melinex) for the energy range from about 0.05 MeV/nucleon to 1.0 MeV/nucleon (16 MeV ^{16}O). It is important to appreciate that the upper energy limit is not specially significant in practice because the particle is continually losing energy as it burrows into the detector. Hence a ^{56}Fe particle with 300 MeV/nucleon will not initially leave a track in polycarbonate (Lexan). At some depth below the surface its energy will have been cut back to about 70 MeV/nucleon at which point it will be moving slowly enough so as to begin leaving a track. The etching of such a track cannot be immediate and there will be an incubation period during which the undamaged surface layers are dissolved before the etchant has access to the track. Of course, if the detector is in the form of a thin film and the particle has sufficient energy to achieve complete penetration, then etching will commence immediately at the back surface.

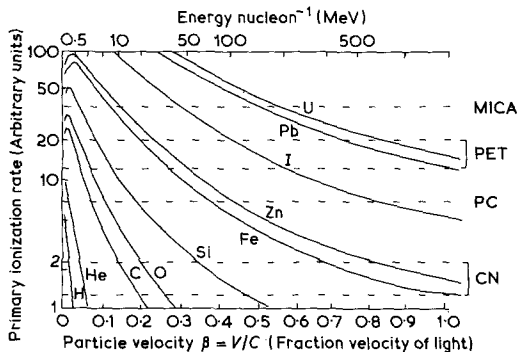


Figure 2 Detection thresholds of four types of track detector for particles of increasing atomic number and energy. The horizontal lines represent the values of primary ionization rate which must be exceeded for etchable tracks to form. Note that the damage density increases as the particle slows down. PET = polyethylene terephthalate; PC = polycarbonate; CN = cellulose nitrate. (Adapted from [1].)

Another sensitivity sequence is given in Table IV [10]. For each material the lightest detectable particle is listed, in addition to the critical energy loss rate $(dE/dx)_c$ necessary if a particle is to leave a track. The parameter $(dE/dx)_c$ varies with particle energy in a manner similar to the primary ionization rate plotted in Fig. 2, and the critical

TABLE IV Sensitivity sequence [10] for ion detection in SSNTDs

Material	Critical rate of energy loss* (dE/dx) _c (10^7 MeV m ² g ⁻¹)	Lightest detectable ion	Atomic no. Z
Procene	20	Ca	20
Zircon	19	Ca	
Tektite glass	15	S	16
Quartz	15	S	
Mica	13	Si	14
Polyester resin	4	O	8
Polycarbonate	4	C	6
Cellulose acetate butyrate	2	He	2
Cellulose nitrate	2	H	1

* The rate of energy loss is a damage parameter related to primary ionization rate, its units are based on it being the energy loss/metre of track length/unit density of detector material.

energy loss rate for a particular material has much the same meaning as the horizontal lines on the figure.

Cellulose nitrate is the most sensitive detector material in wide use. It can record protons in the energy range 0.02 to 2.2 MeV [11] although its efficiency drops off noticeably below 1 MeV. Recent work [12] has shown the cross-linked polymer resin allyl diglycol carbonate to be more sensitive than cellulose nitrate.

The existence of a lower energy below which no track is formed means that the track will often terminate before a particle finally comes to rest in the material. The distance between the end of the track and final particle position is known as the range deficit.

3. The damage process

The narrow trail of damage caused by an energetic particle penetrating some distance into a solid is illustrated schematically in Fig. 3. It is possible to divide the damage process into five sequential stages:

- (1) electrons are stripped from the penetrating particle;
- (2) the region in which the particle is moving too fast to leave damage;
- (3) the main region of etchable damage;
- (4) the stage during which the particle still penetrates the solid but does not produce significant damage;
- (5) the point at which the particles come to rest which may be preceded by a short second region of damage.

Not all these stages are necessarily apparent. Stage 2 will only be present if the particle enters

the recorder at too high an energy. Frequently, especially in the case of polymers, stage 4 cannot be observed and the main damage region merges with that characteristic of stage 5, the track being continuous right up to the range limit.

In this section the various mechanisms which are thought to operate in the different stages will be reviewed. Their nature depends on the type of material and in general known SSNTDs fall into

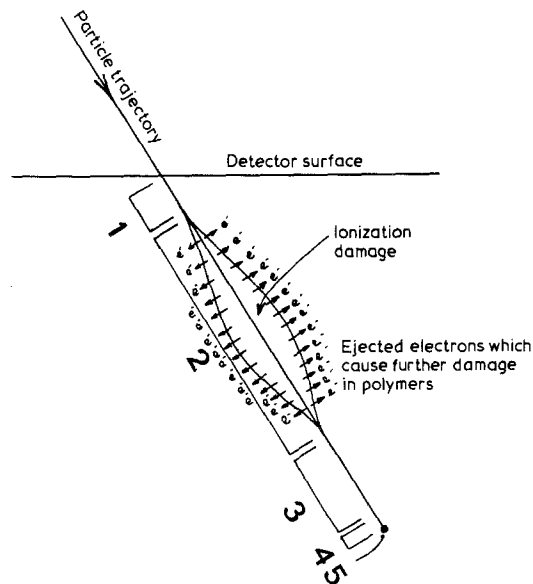


Figure 3 Schematic diagram representing the different stages of penetration of a particle into a detector. Not all the stages are necessarily apparent for a given set of conditions. Stages: 1, Electrons are stripped from particle. 2, Particle moving too fast to leave etchable damage. 3, Main region of damage. 4, Particle regaining electrons and damage no longer etchable. 5, Some elastic collisions as particle comes to rest which may cause damage if particle is heavy.

two distinct categories: organic polymers on one hand and inorganic glasses and crystals on the other. Several organic polymers can record particles at energy loss rates less than $4 \times 10^7 \text{ MeV m}^2 \text{ g}^{-1}$ (energy loss/metre/unit density) while cellulose nitrate will record at energy loss rates as low as $1 \times 10^7 \text{ MeV m}^2 \text{ g}^{-1}$, which enables protons to be detected. On the other hand, inorganic detector materials are not capable of recording at energy loss rates less than $15 \times 10^7 \text{ MeV m}^2 \text{ g}^{-1}$. Accordingly, it is not surprising that the atomic mechanism of damage is different in the two classes of material.

The damage process will be described with two different systems mica/280 MeV ^{56}Fe and polycarbonate (Lexan)/280 MeV ^{56}Fe as examples.

3.1. Stage 1: electron stripping

A particle penetrating a detector will interact with the atoms of the material over its entire range. This interaction may not produce damage of sufficient density to render the track etchable over the full range. A particle, which can be atom or ion, will initially lose some or all of its electrons by virtue of their interaction with the electrons of the detector material. The degree to which the particle will be ionized can be estimated from the equation of Heckman *et al.* [13]

$$Z^* = Z [1 - \exp(-130\beta/Z^{2/3})] \quad (1)$$

where Z^* is the number of electrons removed from the particle, i.e. its net positive charge, β is the initial velocity (as a fraction of the velocity of light) of the particle, and Z is the atomic number of the particle.

For 280 MeV ^{56}Fe particles, which have a velocity of 0.32 that of light ($\beta = 0.32$), $Z^* \approx Z$, which means that the particle loses all its electrons on entering the detector material. The particle thus proceeds as Fe^{26+} , the iron nucleus. Under these conditions it is not surprising that the material will respond virtually identically to incident atoms and lightly charged ions of the same element.

3.2. Stage 2: penetration at velocity too great to leave etchable track

Reference to Fig. 2 shows that 280 MeV ^{56}Fe particles ($\sim 5 \text{ MeV/nucleon}$) leave tracks in polycarbonate at their full energy. Hence the track will commence at the detector surface and stage 2 will be absent.

On the other hand, in mica, which has a higher

damage threshold, the ^{56}Fe particles are initially moving too fast to create etchable damage and stage 2 will continue until their velocity is reduced to $\beta \approx 0.15$ where the track begins. The fact that no etchable track occurs on initial impact in mica does not mean that there is no damage trail, rather that the damage is not continuous enough to provide a preferential etch path. Fleischer and Price [14] state that in the case of mica a track will not be etchable unless the damage is atomically continuous. In a later paper [6] they equate this with the necessity of ionizing at least one mica atom per atomic plane traversed. In polymers it is likely that mechanisms exist which can propagate damage from the track centre line and hence the primary ionization density required for etchability will be significantly lower. We have here a simple-minded suggestion as to the greater sensitivity of polymers as track recorders, which will be developed in greater detail later (Section 4).

3.3. Stage 3: the main regions of damage

This stage commences at the point at which the particle is moving slowly enough to provide sufficient damage density along its path. With 280 MeV ^{56}Fe this is coincident with the surface for polycarbonate but below the surface for mica. Stage 3 terminates when the penetrating particle has slowed and regained electrons to the extent that it is no longer sufficiently potent to create the damage density necessary for track etchability.

(We propose to describe here the main damage processes for the two main classes of material on the basis of the most widely held explanations while deferring a fuller appraisal of the different theories to the next major section.)

Considering first the example of 280 MeV ^{56}Fe in mica, we will look at the damage in terms of the ion explosion spike mechanism proposed by Fleischer *et al.* [6]. The highly charged iron nucleus collides with mica atoms imparting energy to them which is mainly absorbed in the excitation of electrons. A proportion of electrons will be ejected from the atoms and penetrate the surrounding material. They are known as δ rays or bremsstrahlung (braking) electrons. In mica and other inorganic dielectrics the δ rays themselves produce little additional damage. However, the atoms which have lost electrons, grouped as they are down the path of the iron nucleus, will recoil from each other as a result of their mutual Coulomb repulsion. The process is illustrated in Fig. 4. It is this linear con-

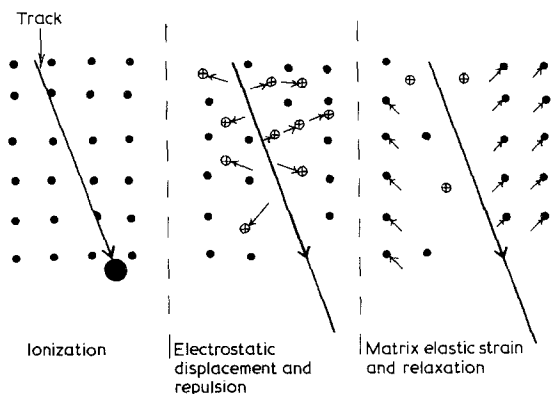


Figure 4 Stages of the ion explosion spike mechanism for track formation in inorganic dielectric solids. The impinging particle ionizes atoms in its path which undergo mutual electrostatic repulsion. Despite some subsequent relaxation, the atomic displacements lead to an etchable track.

centration of damage due to the “ion explosion” which forms the etchable track. It appears that the damage along the track in an inorganic insulator is not continuous but that highly damaged regions alternate with ‘islets’ of little damage [15].

In the case of the polycarbonate, whose behaviour is fairly typical of all the polymers, damage mechanisms are available in addition to the ion explosion spike. Polymer molecules can be degraded at energies below that required for ionization. The formation of free radicals can lead, via various radiochemical processes to chain scission (drastic reduction of molecular weight), the degradation of side groups into low molecular weight species and the formation of cross links. The first two of these mechanisms, in particular, lead to enhanced dissolution rates. The lower energies necessary for polymer degradation mean that the δ rays also contribute significantly to the damage in their own right leading to enhanced etching rates comparatively remote from the track core in which the ion explosion mechanism predominates.

3.4. Stage 4: particle track no longer etchable

There is a minimum velocity below which damage is insufficient to produce an etchable track. It is indicated by the down-turn of the curves of Fig. 2 near the left-hand edge of the diagram and will be larger for detector materials with low sensitivities. For ^{56}Fe particles in mica, the distance corresponding to stage 4, which is called the range deficit, where the particle is still moving but leaving no track, has been measured as $1.2\ \mu\text{m}$ [16], a distance

barely resolvable by the light microscope. In the case of polycarbonate and plastics in general, stage 4 is not apparent and no range deficit is measurable.

3.5. Stage 5: termination

The reason why the end of the track is designated stage 5 is because it has been proposed that a different damage mechanism operates as the particle, probably with its complete complement of electrons regained, finally comes to rest. The mechanism is seen to be the production of atomic displacements due to atom-particle collisions. Calculations [1] indicate that for polycarbonate, etchable damage would occur over the final $0.2\ \mu\text{m}$ of the range and would overlap the ion explosion/ δ ray primary mechanism. In mica, elastic collision damage would be confined to the final $\sim 0.1\ \mu\text{m}$.

Tracks which consist solely of stage 5 can occur for heavy particles (^{56}Fe and above) of very low energies $\sim 1\ \text{keV/nucleon}$. They have been reported for heavy fragments from alpha decay of heavy nuclides [17] and for solar wind particles [18, 19].

4. Theories of track formation

The physics of the interaction of energetic atomic particles with solids was well established before the first documentation of etchable tracks in dielectrics in 1958 [3]. Three models of the radiation damage mechanism are pertinent to the understanding of track formation. They are: atomic displacement, thermal spike, and lattice instability. The first two were discussed at an early stage (1949) by Seitz [20]. The displacement damage occurs in a localized region in which atoms have simply been knocked from their original positions by the penetrating particle. In a crystal, the nature of the damage is easy to envisage as a high concentration of point defects. On the other hand, a thermal spike is seen as damage that is the direct result of intense local heating which melts the material along the particle track, the subsequent very rapid quenching leading to a defective material. As with the atomic displacement model it is more simple to understand this mechanism in the case of crystalline materials, although the suggestion by Bullough and Gilman [21] that the damage should be viewed as a region of thermally induced internal stress would be equally applicable to non-crystals. The term “spike” is used to imply a concentration of

damage at the end of the track as is predicted by the model.

The lattice instability model is due to Varley [22, 23]. Basically the idea is, that when a penetrating particle causes like ions to be adjacent to each other, subsequent damage can result from their mutual repulsion. Originally the juxtaposition of ions was seen in terms of displacements in ionic crystals. It is also the basis of one model of the sputtering process in which the impacting ion ionizes the surface atoms by electron ejection and is followed by the expulsion of the charged atoms due to mutual repulsion [24, 25].

There are several characteristics of etchable track formations in solids which give clues to the most probable mechanism. These are:

(a) etchable tracks are not formed in good electrical conductors and have never been seen in metals;

(b) the etchable damage is fairly evenly distributed along the track, and frequently there is a range deficit in the less sensitive detectors;

(c) tracks are observed in both crystals and non-crystals.

Characteristics (b) and (c) appear to rule out the thermal spike mechanism in which the damage is concentrated at the end of the track and which is only clearly viable in the case of crystalline materials. Furthermore, the linear disposition of damage and the observation of range deficits are not compatible with displacement models which envisage a "spike" distribution [32]. However, the characteristic which most clearly points to a lattice instability model, is the absence of track formation in metals. It is impossible to explain in terms of the atomic displacements models why damage should occur in fairly soft plastics on one hand and very hard minerals on the other, but not in metals of intermediate binding strength. The most basic characteristic of a metal is the presence of highly mobile (free) electrons, and it is not difficult to see that in the case of the lattice instability mechanism they can provide a virtually instantaneous electron repair kit, so ions created by the penetrating particle cannot remain as such long enough for the mutual repulsion stage of the damage to have any effect.

Recognizing such an argument, Fleischer *et al.* put forward their ion explosion spike mechanism in 1965 [13]. The theory, which is illustrated in Fig. 4 and was outlined in the previous section, is a more general statement of the lattice instability

model of Varley [22, 23] which was, in fact, alluded to by Young in that first track etching paper [3].

For inorganic solids, the ion explosion mechanism provides a comparatively complete explanation for track formation. The penetrating particle ionizes atoms in its path, which then become displaced due to mutual coulombic repulsion. The line of deranged ions forms a preferential path for etchant attack. The electrons driven off as δ rays are absorbed by the material remote from the track. Just to what extent the deposition of energy from δ rays produces additional damage in non-polymeric dielectrics such as minerals remains a matter of conjecture. However, the particular view of Katz and Kobetich [26] that δ rays are immediately responsible for the etchable damage in all detector materials is still maintained [27].

Minerals often consist of crystals which are large compared with track dimensions. In such situations the crystallographic orientation influences the track registration properties [28–30] and the use of such tracks to identify particles is further complicated by the fact that they are faceted in accord with the crystal symmetry. Fig. 5 [31] shows such a track in gadolinium gallium garnet. This is a synthetic material that has been developed such that the track etch rate can be controlled by substituting additions of calcium, magnesium and zirconium.

Although organic polymers are much more sensitive as track recorders than the inorganic dielectrics, there is every reason to suppose that the primary mechanism of damage remains the ion explosion. The difference in the case of polymers

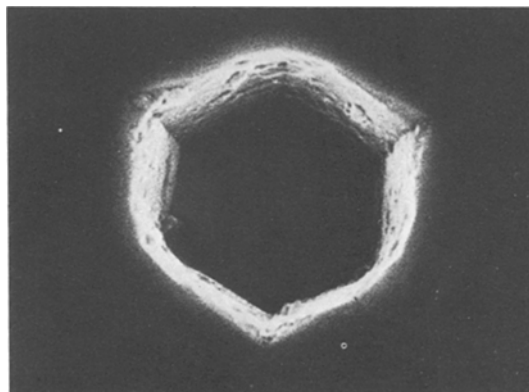


Figure 5 SEM of a track made by $6.72 \text{ MeV amu}^{-1} {}^{235}\text{U}$ ion at vertical incidence on a $\{111\}$ face of pure Gd–Ga garnet. The influence of crystal symmetry on the shape of the track is clearly apparent [31].

is that etchable damage can be created by chemical changes (radiochemical damage) in addition to atomic displacements, and the chemical changes can be induced by electronic excitations which require less energy than ionization events. In addition to the ion explosion effect, the penetrating particle will create excited electronic states over a somewhat larger range than direct ionization. Furthermore, the δ rays produced by the primary ionization can themselves damage polymers radiochemically, and because of their range, they cause the region of etchable damage to be less localized around the particle path. That electrons induce chemical changes in polymers is well known, particularly as beam damage during, for example, scanning electron microscopy [33] and the effect is exploited in the technology of electron-resists. Calculation has shown that localized dosages of Mrad proportions are possible for low energy δ electrons adjacent to particle tracks [26, 34, 35]. (It is also generally true that gamma irradiation enhances the bulk etching rate of polymers [36, 37].)

Higher energy δ rays can deposit their energies through the bulk material and may not directly promote the formation of a track. In polymers, the "threshold energy", below which etchable damage can occur, is often related to a critical dose in the region surrounding a track. Monnin [34] has calculated the diameter of this region to be approximately 100 to 200 nm for α -particles in MeV range. For example, in a polycarbonate, only secondary electrons with energies less than 100 eV can deposit significant energy in the etchable portion of the ionizing particle track. The total radiochemical energy imparted to a system is accounted for by three effects: (1) ionization (energy for polymers 9 to 15 eV); (2) excitation (energy about 6 eV); (3) vibration (energy less than 6 eV). These contributions to total energy have been calculated by Fain *et al.* [35] and are given in Fig. 6 for cellulose nitrate. Mozumder [38] has also discussed the electronic processes of track formation in its early stages. When δ rays are produced, the higher energy ones, as a consequence of their considerable range, deposit their energies throughout a large volume of the bulk detector. Etchable damage will occur in the regions immediately surrounding the particle trajectories if a threshold dose of $\sim 10^6$ to 10^7 rad is exceeded. Only secondary electrons with energies less than a few hundred eV can deposit substantial amounts

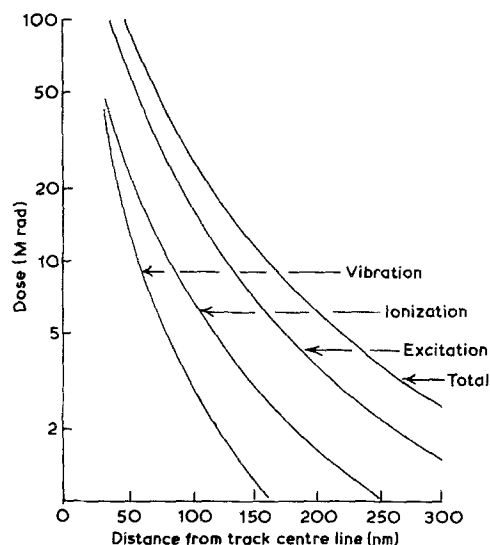


Figure 6 Calculated contributions of excitation, ionization and vibration to total energy as a function of distance from the track centre line for an initial period of 10^{-13} sec. The detector material is taken as cellulose nitrate and the incident particle as 0 to 8 MeV nucleon $^{-1}$ He. (Adapted from [26].)

of their energies within the etched track region of an ionizing particle. It is useful to note that the range of a 100 eV electron in polymers is estimated to be ~ 0.2 to $0.3 \mu\text{m}$ while the diameter of the region in which above-threshold doses occur has been calculated to be between 0.2 and $1.0 \mu\text{m}$ for alpha particles up to several MeV in energy.

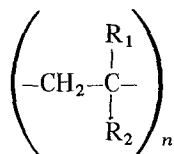
Excitation events will also occur as the result of electron-ion recombinations.

4.1. The nature of damage in polymeric track recorders

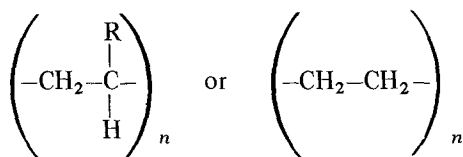
Radiation damage in polymers normally involves scission (cutting) or cross-linking of the molecular chains. The reduction of molecular weight by scission enhances the rate at which the polymer will dissolve and most of the more sensitive polymeric track detectors will degrade by this mechanism. However, tracks have been observed in polymers such as polyethylene (cf. Table II) which degrade by cross-linking. This suggests that the etch does not operate by straightforward molecular dissolution, for cross-linking renders a polymer less soluble, but that it chemically attacks the polymer molecule more rapidly in the region of radiochemical damage even though there may be cross-linking. The composition of some of the more successful etches for polymers which degrade by chain scission (they often contain

oxidizing agents) indicates that in this case too, chemical reaction with the molecules plays a part in preferential dissolution. The prediction as to which polymers undergo chain scission and which cross-link when irradiated is made easier by an empirical rule of Muller *et al.* [39].

The rule is that the general structure for polymers which undergo chain scission on degradation is:



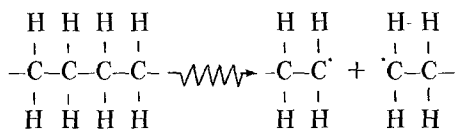
while those which cross-link have the form:



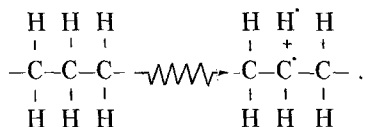
Such a rule, however, does not cover the cellulose derivatives, polycarbonate or polyethylene terephthalate, all of which have ring structures in the backbone and degrade.

Various sources [1, 40, 41] emphasize how little is known about the relationship between physical and chemical properties of polymeric materials and their track-registering capabilities. On the other hand, there is extensive literature on the general radiochemistry of polymers [42-45].

Specific mechanisms have been proposed for radiation degradation. If one considers polyethylene as an example, it is seen that radiation can create free radicals either by breaking C-C backbone bonds:



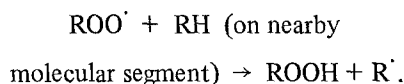
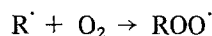
or by breaking a C-H bond:



For polyethylene, the first reaction produces radicals which are likely to recombine, the flexibility of the polymer chain making this more likely in that the broken ends do not have to approach each other in a highly specific orientation before recombination is energetically favourable.

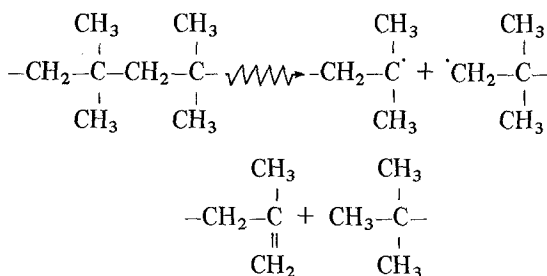
The slightly greater stability of the C-H bond compared with the C-C bond, means that the second radical-producing reaction is a little less likely than the first; however, the high mobility of the hydrogen radical means that recombination is much less likely and the carbon radical will have an appreciable lifetime. Two adjacent radicals on different molecules will combine to create a chemical cross-link, a reaction which is much enhanced if oxygen is present as it provides a mechanism for radical propagation and increases the probability of juxtaposition and hence cross-linking.

The propagation reaction which involves oxygen can be represented as:



The radical has thus propagated from one segment to another.

In doubly substituted molecules, that is those which tend to undergo scission, the probability of recombination between broken chain ends is much reduced, not only because of the greater molecular stiffness but because it is possible to form stable terminal groups [44, 45]. For polyisobutylene, the stabilization of the scission event is seen to occur as:



It has been pointed out by Katz [27] that the damage occurring in polymers is due to a multi-hit process, that is that two or more co-ordinated events are necessary to produce significant damage in the molecule. The evidence for this is that the linear energy transfer as revealed by track etching rate is proportional to approximately Z^4/β^4 (Z is particle atomic number and β its relativistic velocity) and not Z^2/β^2 which would be expected from a one-hit process as is envisaged in the Bethe equation [9].

Thus, in the case of polymeric SSNDTs the damage process has several stages. As with inorganic detectors the passage of a charged particle will cause ionization of the atoms, which will rearrange themselves due to mutual repulsion of like charges. For polymers, however, this very localized damage may not be significant compared with the effects due to the stripped electrons as they are injected into the surrounding material. Some may recombine with the ionized atoms, in which case the energy liberated can create a free radical, the majority, however, will play a part in the direct creation of radicals as they deposit energy during deceleration.

5. Track etching

5.1. Etch-pit geometry

Tracks etch preferentially and can thus be enlarged by chemical action to a size which is visible in the light microscope. The preferential action of the etch is characterized by the ratio v_T/v_G where v_T is the rate of dissolution along the track and v_G the bulk etch rate of the detector surface remote from any tracks ($G \equiv$ general). In the simple instance of a particle penetrating a detector normal to its original surface as in Fig. 7 and assuming that v_T is constant along the track and v_G is constant and isotropic, then v_T/v_G will be constant for short etching distances in isotropic non-crystalline solids.

Both l and d are directly observable quantities from the competitive effects of v_G and v_T and become smaller as v_T approaches v_G and vice versa, i.e. both l and d decrease as v_T/v_G decreases. Hence, for the situation envisaged in Fig. 7:

$$l = (v_T - v_G)t \quad (1)$$

where t = etching time, and

$$d = 2v_G t \left[\frac{(v_T - v_G)}{(v_T + v_G)} \right]^{1/2} \quad (2)$$

It can be seen that when $v_T = v_G$, both l and d vanish, which is a required property of these equations. Also the cone angle, as defined in Fig. 7 is given by:

$$\theta = \sin^{-1}(v_G/v_T) \quad (3)$$

Not surprisingly these three basic equations can be combined and manipulated to give imposing relations which are useful in specific instances.

For the more general case of oblique particle incidence, the geometry is more complicated. The

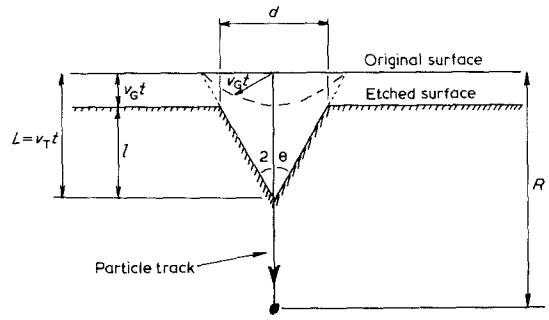


Figure 7 Track etching geometry for the case of a particle impacting at normal incidence.

intersection of the etched track with the major and minor axes (a and b) of the ellipse is displaced such that the track line is not at its centre. The geometric parameters are indicated in Fig. 8 which is adapted from [48] which also contains the relevant relations. Important among these are firstly those which enable the cone angle θ , the track obliquity angle ϕ , and the track length L to be determined from the experimentally measurable quantities: a , p , Z and v_G (cf. Fig. 8).

$$\theta = [-\arctan(Z/(a+p)) + \arctan(Z/p)]/2 \quad (4)$$

$$\phi = [\arctan(Z/a+p) + \arctan(Z/p)]/2 \quad (5)$$

$$L = (Z + v_G t)/\sin \phi \quad (6)$$

The major and minor axes of the elliptical intersection of the etched track with the recorder surface are given by

$$a = 2v_G t (\sin \phi - \sin \theta) \cos \theta \times [\sin(\phi + \theta) \sin(\phi - \theta)]^{-1} \quad (7)$$

$$b = 2v_G t (\sin \phi - \sin \theta) / (\sin \phi + \sin \theta)^{1/2} \quad (8)$$

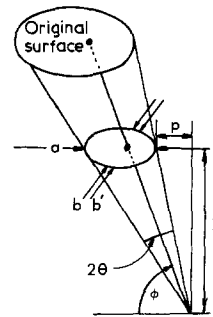


Figure 8 Diagram defining track geometry for a particle at incident dip angle ϕ and constant v_T and v_G . (After [48].)

Equations 7 and 8 demonstrate the condition that $\phi > \theta$ for tracks to be etchable. Bearing in mind that $\sin \theta = v_G/v_T$, the condition can be rewritten as:

$$\sin \phi > \frac{v_G}{v_T}. \quad (9)$$

Hence, for any given v_G/v_T , a ratio dependent on the recorder material, etchant and etching conditions, and the degree of damage in the track, there will be an obliquity beyond which no track can be revealed by etching. In other words, if the component of v_T in the direction normal to the recorder surface is less than v_G , there will be no preferential etching and hence no visible track. The fraction of solid angle over which tracks are etchable is $(1 - \sin \theta)$ and this parameter is equal to the etching efficiency, that is the fraction of tracks intersecting the surface which can be revealed, for situations in which the incoming particle flux is independent of orientation. For recorders which are thicker than the track length there is a measure of discrimination against highly oblique tracks at long etching times, as they terminate at positions nearer to the recorder surface than tracks of more normal incidence. Thus on etching a thick recorder containing tracks of finite length but random orientation, the number of tracks apparent will remain constant until the depth just below the ends of tracks with an obliquity $\phi = \theta$. Etching of sections below this depth will, technically, take place with 100% efficiency but the number of tracks appearing will decrease and finally become zero at a depth corresponding to the track length.

Table V from [49] shows values of the etching efficiency.

Several workers have taken part in the development of the appropriate geometric equations to describe etch-pit formation. There is a notable list in [1]; however, probably the most comprehensive as well as the clearest presentation of the geometry of track etching is given by Ali and Durrani [50].

The geometry of the etched track becomes more complicated if v_T varies along the track length, and this more realistic situation has been treated by Fleischer *et al.* [51]. In general terms, an increasing v_T with depth will produce a cone of increasing sharpness, the surfaces being concave from without, while a decreasing v_T will give the opposite effect, although the cone point

TABLE V Detection efficiency and critical detection angle of various SSNTDs [49]

Material	Etching efficiency for isotropic (2π) incidence (%)	Minimum angle of incident for detection
Polycarbonate	95.7	2° 30'–3.00°
Mica	92.0	4° 30'
Quartz	87.5	7° 15'
Tektite glass	56.8	25° 45'
Obsidian glass	56.7	26° 00'
Soda-lime glass	42.3	35° 30'

remains sharp until v_T has decreased virtually to the bulk etch velocity of v_G .

A very considerable volume of work has been carried out searching for suitable and improved etches for recorder materials. It is likely that many details of particular trials remain unpublished, but notwithstanding, the literature on the topic is considerable and would consume inordinate space if reproduced here. The reader is referred to the table on pp. 65–72 of [1] for the most comprehensive listing of satisfactory etchant/recorder combinations currently available.

5.2. Factors influencing etch rate

5.2.1. Etching conditions

In principle, any chemical reagent will function as an etchant if it attacks a detector at an appropriate rate, and usually etching conditions are optimized empirically for each detector material. For minerals and glasses many etches are based on hydrofluoric acid; however, solutions developed to give dislocation etch pits in inorganic crystals [52] often prove to be good choices for revealing nuclear tracks. Etches used for polymers are often formulated such that they degrade the polymer molecules, that is cut them, and then dissolve away the lower molecular weight debris. It may well be that it is the degradation step which is enhanced by the radiation damage, and this point is emphasized by the fact that polymers which cross-link under radiation can be etched to give tracks and also that the recently reported very sensitive polymeric detector, allyl diglycol carbonate, is itself a cross-linked material [12, 53]. Etchants from polymeric detectors are frequently solutions of alkali hydroxides although many contain specific oxidizing agents such as potassium permanganate or potassium chromate. Not surprisingly there have been many investigations of experimental etching parameters for the more

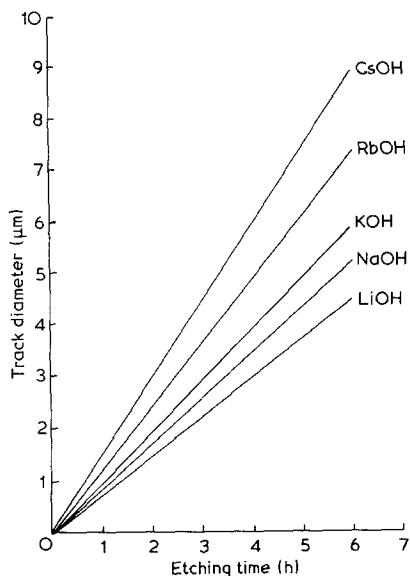


Figure 9 The effect of alkali hydroxide type on the track etching rate of a polycarbonate. 5 N solutions of 60° C. (After [43].)

common polymeric detectors [54–64]. These have elucidated the influence of composition of the etch, its strength, its temperature and also degree of liquid agitation and various pre-etching treatments on the development of track pits. Figs. 9 and 10 are examples of this extensive data. The reason why alkalis based on the larger, heavier, ions appear to etch more rapidly can be understood when the radius of the ion together with

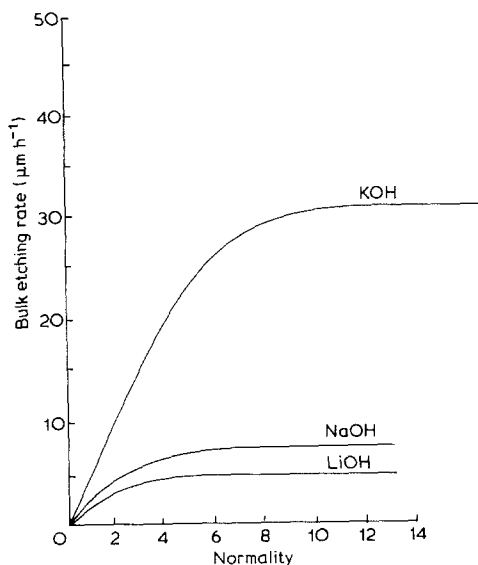


Figure 10 The effect of etchant concentration on the bulk etching rate of a cellulose nitrate detector (Daicell) at 50° C. (After [54].)

its cluster of water dipoles is taken into account. The greater rate of penetration achieved by the heavier ions is due to the fact that they collect less associated water molecules than lithium and sodium and are thus in effect, smaller [65]. Latterly, a surfactant has been included in many etchant compositions [57] presumably in attempts to lower the surface free-energy between polymer and etchant, achieve better wetting and hence a more uniform chemical attack.

5.2.2. Environmental effects after irradiations but before etching

Polymer surfaces on exposure to photo-radiation undergo various changes, either alone or in combination, usually of oxidative, ozonolysis, or thermal character which cause chain scission and/or cross-linking. Such effects lead to either localized or bulk surface hardening, or softening, dependent on the dominant reaction in any specific instance. Surface “hardening”, often caused by heating or ageing, is usually associated with a decrease in etching rate, while “softening” can cause a substantial increase. “Softening” agents observed, in addition to ultraviolet light [58, 66, 67] have been O_3 [58, 68], H_2O_2 [69], NO [70]. The moisture content of some detectors, as indicated by their storage humidity conditions, can also affect the etching rates of a water-sensitive polymer, e.g. cellulose nitrate can be made to double its etching rate [71]. It has also been reported that the storage of polycarbonate in liquid nitrogen prior to etching increases its sensitivity to α particles [73].

A neutral environment of vacuum or nitrogen atmosphere decreases the track etching rate, possibly by oxygen exclusion. It is useful to note that the detector cellulose triacetate irradiated in a vacuum will not display alpha particle tracks on etching but can be sensitized after exposure to oxygen at high pressure (≈ 100 atm) [1].

Cellulose nitrates, polycarbonates, polyethylene terephthalate all show increased track etching rates on exposure to O_2 , NO , H_2O_2 + ultraviolet light. Exceptionally, N_2O + ultraviolet decreases track etching rates.

The experimental consequences of these facts are that polycarbonates, after irradiation, need protection from ultraviolet light sources such as sunlight and fluorescent lights if it is important that their track etching properties be standardized. Cellulosics after irradiation need oxygen aeration, atmospheric pressure being satisfactory followed

by either prompt processing, or refrigeration, to suspend any chemical changes as in this instance the etch rate slowly decreases with time and gradual polymer decomposition occurs.

The various additives, anti-degradants, plasticisers, etc., used in formulating polymer materials often considerably change their etching characteristics, rate variations of 1 to 35 have been reported [63, 72]. In particular, the presence of an ultraviolet stabilizer is recognized as suppressing the track-etching properties of polymeric detectors by conferring opacity to ultraviolet light.

In the case of crystalline materials, high doses of lightly ionizing radiation have so far failed to alter measurable etching parameters. However, weathering [74, 75], specific annealing [76], and other thermal effects [77], do play influential roles in the etching of tracks in inorganic detectors.

5.2.3. Thermal history

It is possible to erase latent tracks by suitable thermal treatment below the melting point or decomposition temperature of the detector. The effect was first seen in polycarbonate [78] but it has since been established as a general phenomenon pertaining to both polymeric and inorganic detectors, [6, 79, 80]. Two observations concerning the annealing of tracks are particularly significant. Firstly, the process is thermally activated in that a combination of time and temperature is necessary to achieve the effect. It is possible to measure an apparent activation energy for the process which is typically that for atomic diffusion in the detector. Secondly, and perhaps not surprisingly, the track is erased more rapidly where the linear energy transfer, and hence damage, is less and close to the surface. Thus the etching response which is measured in order to identify the particle is also effected by the thermal history (cf. Section 6.2). This is significant where one is etching, for example, lunar or meteoritic material in order to determine its bombardment history over periods on a cosmic scale. The detector material cannot be calibrated without knowledge of its thermal history, and even if this is known, it is still necessary to extrapolate the activation plot to low temperatures and very long time. However, if more can be assumed concerning the nature of the radiation, cosmic rays for example are rich in iron ions, then the track-etching characteristics can be used to give some indication of thermal history.

Table 2.4 of [1] gives a detailed listing of the

TABLE VI Some thermal track fading characteristics of polymers [1]

Polymer	for: 1 h annealing; temperature (° C)		
	Total fading	50% track loss	Start of track loss
Cellulose acetate	165	~ 160	> 100
Cellulose nitrate	138–147	85–130	> 110
Polycarbonate	185–200	170–190	100–110
Amber	–	110	–
Natural quartz [86]	–	–	> 950

various reported (to 1975) annealing effects. Table VI adapted from the same source, in addition to giving some typical temperatures, shows that track fading is a progressive phenomenon with some tracks being lost before others.

6. Application

6.1. Measurement of particle flux

Etching renders particle tracks visible in a light microscope, so a measurement of dose basically involves counting of etched tracks. Various techniques have been devised to either improve the visibility of the etched tracks and/or to automate their counting.

6.1.1. Techniques to improve track visibility

(i) Polarized light and the use of a crossed polarizer can enable the light scattered from track surfaces to be detected [82, 83].

(ii) A thin 8 to 12 μm layer of red-dyed cellulose nitrate is coated onto a less sensitive base of polyester film. Etched tracks appear as holes against a red background which can be enlarged and permanently recorded on high contrast film or photographic paper [84, 85].

(iii) The light guide principle is used to reveal tracks in SSNTDs by using a fibre optic to introduce light at the edge of a detector through light-tight jaws when the trapped illumination escapes from the surface when a hole is encountered. The resulting effect is a field of bright tracks on a dark background [86].

The following methods seek to fill tracks with various opaque substances.

(iv) The etched surface of the detector can be silver coated and the nuclear tracks made visible by reflected light to assist counting purposes [87].

(v) It is arranged that when a track perforates the detector it reacts with chemicals in an underlying indicator material so as to produce localized absorption spots [88].

(vi) A fluorescent dye can be used to penetrate etched tracks which are then viewed using ultraviolet light [82].

(vii) The etched holes in a detector are exposed simultaneously to HCl gas on one side and NH₃ gas on the other, producing white NH₄Cl crystals at each hole [89].

In addition, efforts have been made to reduce the background due to α particle recoils [90] and also generally enhance the surface quality of the film. Pre-irradiation annealing of cellulose nitrate for 48 h at 90°C has been used to improve the evenness of bulk etching and hence aid track counting [91]. Visual track counting is, however, usually a tedious and lengthy procedure and automatic techniques are desirable when speed, high accuracy, evaluation of many detectors or of large areas is required.

6.1.2. Non-microscopic methods of track counting or estimation of dose

(i) Ammonia gas is allowed to penetrate through the etched perforations in a detector and recorded on Ozalid reproduction paper on which the resulting image is enlarged either by projection through a microfilm reader, photographic enlarger, or slide projector permitting rapid scanning of large areas [92].

(ii) A detector is coated on one side with an aluminium film and etched on the other side. The reagent first etches the track and then the aluminium giving transparent apertures 0.1 to 0.5 mm diameter [93]. An alternative is to coat the detector with silver resistant to NaOH, etch the detector with NaOH as normal and then create holes in the silver film with nitric acid attack producing more uniformly sized holes.

(iii) Optical densometric techniques are possible whereby the amount of scattered light is measured proportionally between etched and unetched surfaces [94, 95] and this can be accentuated by means of a red dye [96]. These methods are specially suitable for high track densities where the change in the etched detectors' surface can be seen directly.

(iv) Fraunhofer-diffraction in which a 1 mW He-Ne gas laser as light source is used to measure the average etch pit diameter [97].

(v) Polymer grafting [98] as a means of detecting charged particles has been ingeniously developed in which the high concentration of reactive chain ends and free radicals along the radiation tracks in a polymer, cellulose triacetate, are used to initiate polymerization of a monomer, propenoic acid, to give a cellulose triacetate-propenoic acid graft copolymer. The co-polymer can then be dyed with rhodamine B because of its acid and hydrophilic properties and the tracks seen using fluorescence microscopy. 100% detection efficiency has been reported with ²⁵²Cf fission fragments.

(vi) One observation of the use of a photochromic material as a detector of heavy particles has been made [99] in which strontium titanate crystals containing 0.1% iron as a detector are subject to 1000 V electric field between a uranium foil and detector. Illumination reveals slots of 10 μ m diameter in the detector attributable to alpha particle tracks.

(vii) Alpha particle penetration through a perforated detector can be used as an indicator of total hole area. A scintillation detector on the reverse side of the SSNTD exposed to the high energy particles being used as a measurement device [100, 101].

(viii) Dark-field illumination will cause tracks or etch pits to appear bright against a dark background and the total light scattered into a microscope objective is measured by a photomultiplier placed in the eyepiece [102].

In all techniques based on the measurement of macroscopic effects instead of individual track recognition, the optical density depends on both track density and etching time.

6.1.3. Automatic track counting techniques

These have been recently reviewed [103] and presently form two distinctive classes based on microscopy linked to a TV computer and spark counting procedures; both are appropriate where track density determination is of primary interest.

(i) Scanning microscope instruments, such as the Quantimet Microscope System, have been favoured in which the magnified image of a sector of the detector (the microscope's viewing field) is projected onto the photocathode of a TV tube and scanned and analysed [104-108]. The track counting errors are of the order of 1% and track diameters can be measured to within 5%. Tech-

niques based on this principle have reached a considerable degree of automation.

(ii) The spark counting technique [109–117] is simple in concept and functional capabilities and the most rapid and accurate for low to medium track densities up to $\sim 3000 \text{ cm}^{-2}$ over a relatively large area. An SSNTD in the form of a thin film, about $10 \mu\text{m}$ thick is washed, etched and dried and placed on a flat electrode plate, covered with a piece of aluminized polyester film, metallized side adjacent to the SSNTD and connected to an outer earthed electrode. A positive voltage of about 500 V is applied to the thin aluminium layer causing sparks to occur through the ~ 2 to $10 \mu\text{m}$ diameter perforations in the etched film, and these individually evaporate aluminium from the coating adjacent to the appropriate detector hole. Each spot from which the aluminium has been evaporated is several times larger than the original hole with a typical diameter of 0.2 mm. The circuit is then broken at that hole preventing multiple sparking and leaving a visible replica on the aluminized polyester which provides a map of track distribution in permanent record form.

6.1.4. Use of SSNTDs as particle counters

There are many applications in which counters based on SSNTDs have advantages over the more traditional Geiger–Muller type device. The advantages are frequently those of convenience, the intrinsic compactness and lightness of the SSNTD commending it in fields such as cosmic ray detection in space missions and personal dosimetry. When one considers that the solid state detector both records and stores information for future analysis, the real gains in terms of convenience are seen in even better light. Furthermore the ability to calibrate the detector so as to make particle identification possible (see Section 6.2) enables experiments to be carried out which would otherwise not be contemplated.

Stacks of polycarbonate detectors have been flown on space missions and subsequently track analysis has given important insight into the nature of cosmic rays. In one particular experiment on Apollo 17, a polycarbonate detector was implanted under the scalp of a mouse, so that the actual cosmic ray dose received by the brain could be assessed [118].

SSNTDs are possible replacements for the conventional film badges used in certain types of personal dosimetry. An SSNTD placed in contact

with a film of fissionable material such as ^{10}B or ^{235}U can be seen to count tracks caused by products of neutron-induced fission reactions, e.g. $^{10}\text{B}(n, \alpha)$, and hence indicate the neutron flux. Such a neutron dosimeter has the advantage that it is relatively insensitive to β , X and γ radiation, and that a large range of doses can be studied on one recording film [119]. SSNTDs are also used in radon dosimetry [120].

The particular applications in dosimetry are mirrored by other uses in other fields. For example, the existence of radon permeating to the earth's surface can indicate the existence of underground uranium deposits. SSNTDs are buried a few feet below the surface in inverted cups and removed and analysed for α tracks, which are decay products of ^{222}Rn , after a period of 2 to 4 weeks [121, 122]. The arrangement suitable for neutron dosimetry can also be applied to the measurement of reactor flux [106] where the small size of the detector enables measurements to be made at very particular sites, for example, within uranium fuel pellets.

The high resolution of the SSNTD commends it to metallographic applications. α particles from a source such as ^{241}Am are collimated by an amorphous absorber and detected by an SSNTD after transmission through the metal foil to be examined. Defects in the metal scatter the α particles and hence affect the distribution of tracks in the detector. Grain boundaries [123], twin boundaries [124, 125] and dislocations from cold working [126] have all been successfully imaged by this technique.

Distributions of radioactive elements in metals and other materials can be determined by direct contact with an SSNTD [127–131]. Also neutron-induced fission reactions in boron have been used to determine its distribution in steel [132].

6.2. Particle identification

The linear energy transfer rate for a particle entering the surface of an SSNTD depends on the charge and velocity of the particle and will control v_T and hence the depth of etch pit developed under specific conditions. Here, the etch pit depth is assumed to be small compared with the maximum range of the particle. Likewise, the maximum range (R_{max}) of the particle is also dependent on charge (equivalent to mass as the particle is assumed to be fully ionized) and velocity. The two measurable parameters, v_T and R_{max} vary

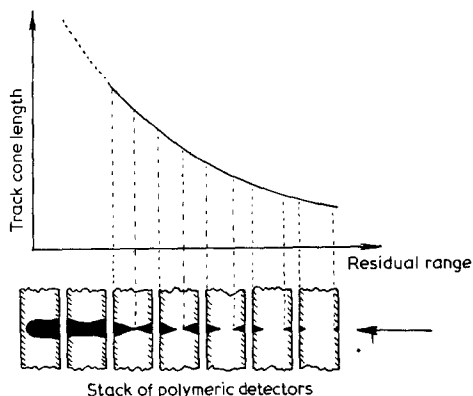


Figure 11 Plot of etched track (core) length L against residual range R measured in a stack of plastic track detector sheets. The particle enters from the right and the residual range is measured from the terminus of the track to the "downstream" end of each etched cone.

independently with charge and velocity and hence a given particle entering the SSNDT under defined conditions will give rise to a unique combination of these parameters. Hence, in principle, if the detector can be calibrated by measuring its response to known ions accelerated to measurable energies, then it can be used to identify unknown particles. Several methods of particle identification are based on this approach. They make use of the fact that the energy of a particle

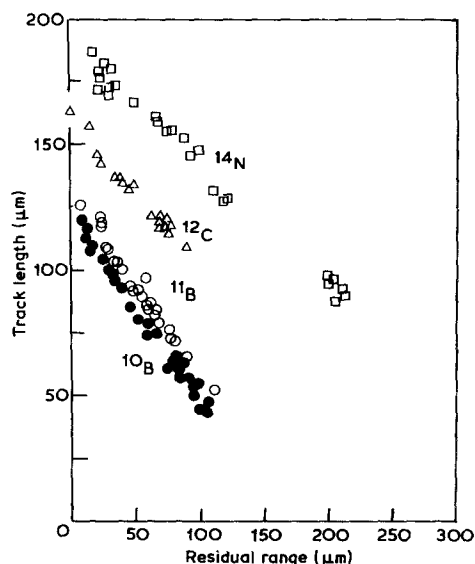


Figure 12 L - R plots for cellulose nitrate exposed to different particles in the energy range 0 to 10.3 MeV nucleon⁻¹ and etched 9 h in 6.25 N sodium hydroxide. Note the resolution of the isotopes of boron (Redrawn from [134].)

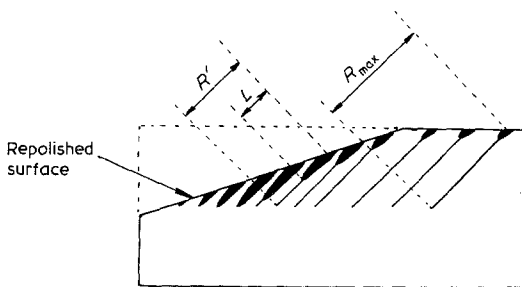


Figure 13 Repolishing technique. R' is the residual range, here measured from the upstream end of the etched track (cf. Fig. 11), L the etched track length and R_{\max} the total range. (Adapted from [136].)

decreases as it penetrates into the detector, so that by measuring v_T at different depths which when subtracted from the penetration R_{\max} gives the residual range R , it is possible to obtain several pairs of values of v_T (or etch pit depth L) and R .

Some of the procedures reported are now reviewed.

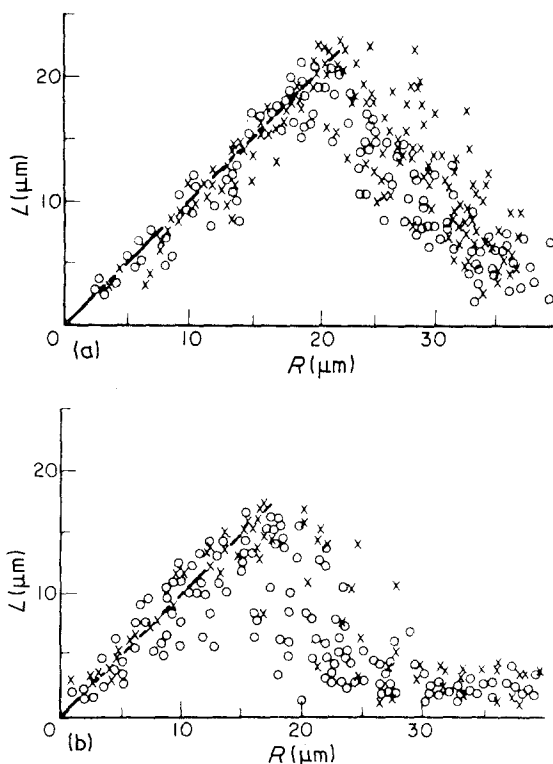


Figure 14 L - R plots for ^{84}Kr particles incident on the mineral bronzite. Data are for two orientations with respect to the cleavage plane ($\times 0^\circ$, $\circ 90^\circ$) and each plot corresponds to a different post-irradiation (but pre-etch) anneal: (a) 450°C, 105 min; (b) 450°C, 130 min. The etch was 60 min in 60% NaOH [136].

6.2.1. Detectors consisting of stacks of polymer film

These detectors can be used in situations in which the particle is able to penetrate several layers. Subsequent etching from each successive interface produces etch pits and gives an indication of v_T at different overall depths along the track. The situation is shown schematically in Fig. 11 [133].

This particular approach was first exploited by Price *et al.* in 1967 [134] and Fig. 12 shows their $L-R$ plots for different ions in cellulose nitrate. It can be seen that the two isotopes of boron are just resolvable. A more recent analysis of the problem of isotope resolution, based on expected errors in measurement of track length [135] indicates that the higher the particle mass the greater the certainty that adjacent isotopes can be resolved.

6.2.2. Repolishing technique

This method is applicable to track measurements

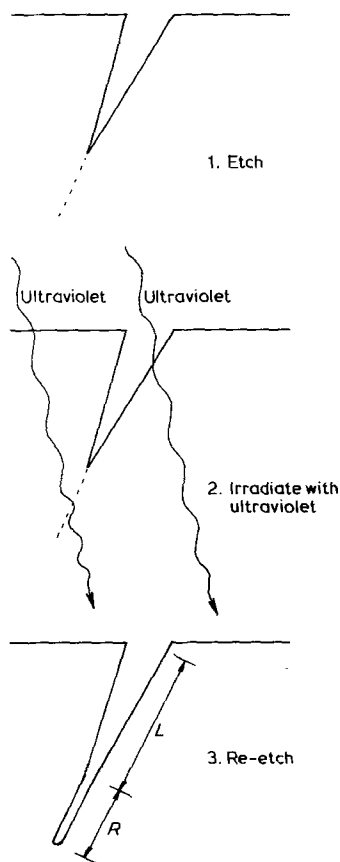


Figure 15 Technique for simultaneous measurement of L and R on a single track in polycarbonate. Ultraviolet irradiation after the first etch increases v_T/v_G so that a second etch leads to a much narrower cone which continues to the end of the track. (After [137].)

in inorganic minerals which (with the exception of the micas) are not available as thin films. The detector material is obliquely reground after exposure but before etching. As can be seen in Fig. 13 [136] it is possible to measure etch pit depths from many different starting points along the tracks. Some $L-R$ plots for the mineral bronzite are shown in Fig. 14 [136]. The first part of the plots where the L and R are equal represents etch pits which have penetrated to the end of the track. The relationship which is of interest as far as particle identification is concerned is that towards the right of the plots. However, owing to inhomogeneity in crystalline minerals, the scatter is often much larger than is seen with stacks of polymeric recorders [84].

6.2.3. Accelerated etch

This is a technique due to Stern and Price [137] which exploits the fact that the track etching rate in polycarbonate is considerably enhanced by ultraviolet exposure after track registration but prior to etching. It enables values of L and of R to be obtained simultaneously for the same track. The recorder is partially etched so as to reveal the tracks, exposed to ultraviolet light and then re-etched sufficiently to allow the etch pit, which is now a much narrower cone, to reach the end of the track. The situation is sketched in Fig. 15. The measurements of original cone depth and range can be made by optical observation or scanning electron microscopy of a replica of the pit.

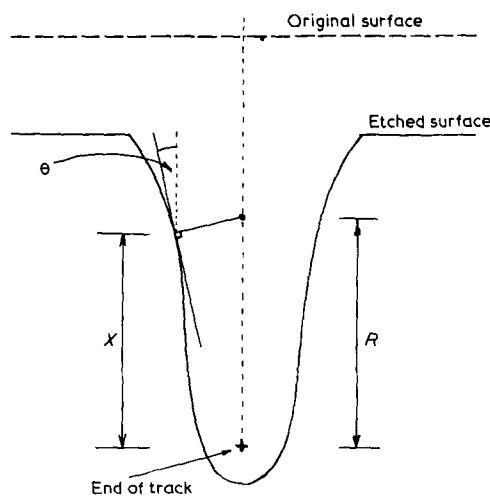


Figure 16 Track profile method of particle identification. $\sin \theta$ at a distance x from the end of the track is equal to v_G/v_T at a distance r from the end. (After [138].)

6.2.4. Track profile

This method applies to tracks which have been etched to the end of the particles' range. The profile of the etched track is not exactly conical but varies as v_T changes with depth. The statement due to Fleischer *et al.* [138] that the sine of the half cone angle at a distance x from the end of the range equals v_G/v_T at the point at which the normal to the wall meets the particle's trajectory, is illustrated in Fig. 16. By using an SEM replica method it is thus possible to obtain a v_T versus R plot from one track and hence identify the particle.

6.3. Production of fine filters

Controlled etching of a thin plastic detector generates holes, the diameter of which can be controlled by specifying etchant and etching conditions while the number is determined by particle dose. Holes of 500 nm are possible and a commercial filter system, Nuclepore [139] is made from the ^{235}U irradiation of polycarbonate film, holes being subsequently etched by immersion in warm NaOH solution [140] and covering the range 3 μm to 8 μm diameter. A number of workers have investigated the parameters and characteristics of these porous membranes [70, 141–145] which have been applied in a diverse number of filtration applications.

It has been observed that 6 μm diameter blood cells, on account of their flexibility, will just pass through 3 μm holes. However, cancer cells are larger and less flexible and it has been established in principle that these malignant cells can be separated by filtering through a track-etched type plastic filter the cancer cells being retained by the filter and thus detectable in a majority of cases [10, 146–149].

The stabilization and clarification of beer and wine is possible through removal of yeasts and their resultant bacteria and sediment by filtration through track-etched filters thus eliminating the pasteurization operation otherwise essential in the production of bottled beer [150].

The practice and theory of track-etched filters for airborne particle sampling and microscopic collection has been reported [48, 151], interesting applications being the sampling of radioactive aerosols [49, 152] and nuclei sampling as low as 10^3 nm diameter used to predict an aerosol's residence time [153].

A single etched track in a film is used as the

basis of a De Blois-Bean Counter which works on the Coulter Counter principle [154]. It has been used to count and estimate size distributions of viruses in suspension [155, 156].

Appendix 1. Glossary of terms associated with nuclear track detectors

Accelerated etching	An increase in the ratio v_T/v_G usually brought about by irradiation with photons after latent track formation but before etching.
amu	Atomic mass unit. Approximately the mass of a neutron or proton: exactly, one twelfth of the mass of a ^{12}C atom.
Annealing	The change or destruction of latent tracks by heat treatment. (The term can obviously be applied more widely and is also used to describe heat treatment of the detector material prior to radiation.)
Cone angle	The semi-apex angle of a conical (or approximately conical) etched track. It is also the smallest particle glancing angle at which a track is capable of being etched.
Delta ray	An electron, ejected from an atom of the detector material, which if sufficiently energetic can produce further damage.
Displacement spike	A region of intense collision damage localized at the point at which a penetrating particle is brought to rest. Only in the case of heavy, low energy particles are displacement spikes considered significant in track formation.
Energy density	The energy deposited/unit track length at a specified distance (e.g. 17 \AA) from the particle trajectory.
Etchable track	Damage along the line of a penetrating particle for which, at a particular intersecting surface, the ratio v_T/v_0 is greater than unity.
Etching efficiency	The ratio of the number of tracks intersecting a given surface which are etchable to the number which would be etchable if all intersections were at normal incidence.
Free radical	An uncharged atom or chemical group which contains unpaired electrons (i.e. unsatisfied bonds).

General etch rate (v_G)	The rate of dissolution of the detector normal to the surface and remote from any track.	Stored energy	The energy per unit length of track which is stored in such a way as to reduce the activation energy for etching.
Ion explosion spike	Damage resulting from the mutual repulsion of atoms ionized by the penetrating particle.	Thermal spike	Damage which can be attributed to intense localized heating and subsequent quenching in the immediate vicinity of a particle track.
$L-R$ plot	A graph of measured track length against the remaining range of the particle. The plot is characteristic for a particular particle type and is used in identification.	TINT	Abbreviation for "Track in Track". A technique whereby large etched tracks derived from heavily ionizing particles, enable etch access to less rapidly etching tracks where they intersect the large ones at positions below the detector surface.
Latent track	A track prior to etching.	TINCLE	Abbreviation for the "Track in Cleavage" technique which achieves the same objective as TINT but exploits cleavage cracks instead of large etched tracks.
Lexan	Trade name for General Electric polycarbonate.	Total energy loss rate	Energy lost by a particle per unit distance.
Nucleon	A nuclear particle which is either a neutron or a proton.	Track	This term tends to be used interchangeably to mean either the latent track (sometimes implied by the phrase "particle trajectory") or the etch pit by which a latent track is revealed.
Primary damage	The removal of electrons from detector atoms or their excitation to higher energy states as a <i>direct</i> result of the close passage of the penetrating particle.	Track enlargement	The deliberate enlargement of an etched track by using dielectric breakdown to assist observations at low magnifications.
Primary ionization rate	The energy loss per unit track length attributable to the production of delta rays.	Track etch rate (v_T)	The rate of dissolution of a detector along the line of a track.
Rad	A unit of absorbed dose equivalent to 0.01 J kg^{-1} .		
Range deficit	The distance which a particle travels before coming to rest <i>after</i> it has ceased to leave a track which will etch preferentially.		
Registration efficiency	The ratio of the number of particles passing through a given surface to the number which produce etchable tracks.		
Residual range	The distance from either the top or bottom of the etched track to the point at which the track is no longer etchable.		
Restricted energy loss rate	The energy loss per unit track length due to the production of delta rays of less than a specified energy (usually 350 eV).		
Secondary energy loss rate	Energy deposited per unit length at a specified distance from the particle trajectory due to delta rays alone.		
Sensitivity	A qualitative measure for detector materials frequently quoted in terms of the lowest primary ionization rate which will lead to track formation or simply the energy and character of the least ionizing particle which can be recorded.		

References

1. R. L. FLEISCHER, P. B. PRICE and M. W. WALKER, "Nuclear Tracks in Solids: Principles and Applications" (University of California Press, Berkeley, 1975).
2. *Nuclear Track Detection*, quarterly (Pergamon Press, Oxford).
3. D. A. YOUNG, *Nature* **182** (1958) 375.
4. E. C. H. SILK and R. C. BARNES, *Phil. Mag.* **4** (1959) 970.
5. P. B. PRICE and M. W. WALKER, *Phys. Rev. Letters* **8** (1962) 217; *J. Appl. Phys.* **33** (1962) 3407.
6. R. L. FLEISCHER, P. B. PRICE and R. M. WALKER, *ibid* **36** (1965) 3645.
7. D. V. MORGAN and L. T. CHADDERTON, *Phil. Mag.* **17** (1968) 1135.
8. J. A. CHAMPION, *Brit. J. Appl. Phys.* **16** (1965) 1035.
9. H. A. BETHE, *Ann. Physik* **5** (1930) 325.
10. R. L. FLEISCHER, P. B. PRICE and R. M. WALKER,

- Science* **149** (1965) 383.
11. G. V. MCKINLEY, *Radiation Effects* **37** (1978) 199.
 12. R. M. CASSON and E. V. BENTON, *Nuclear Track Detection* **2** (1978) 173.
 13. H. H. HECKMAN, B. C. PERKINS, W. G. SIMON, F. M. SMITH and W. BARKOS, *Phys. Rev.* **117** (1960) 544.
 14. R. L. FLEISCHER and P. B. PRICE, *J. Geophys. Res.* **69** (1964) 331.
 15. M. MAURETTE, *Radiation Effects* **3** (1970) 149.
 16. P. B. PRICE, R. L. FLEISCHER and C. D. MOAK, *Phys. Rev.* **167** (1968) 277.
 17. W. H. HUANG and R. M. WALKER, *Science* **155** (1967) 1103.
 18. D. S. BURNETT, C. HOHENBERG, M. MAURETTE, M. MONNIN, R. WALKER and D. WOOLUM, Apollo 16 Preliminary Science Report, NASA Pub. 315 (1972) p. 19.
 19. R. M. WALKER, Z. ZINNER and M. MAURETTE, Apollo 17 Preliminary Science Report, NASA Pub. 330 (1973) p. 2.
 20. F. SEITZ, *Disc. Faraday Soc.* **5** (1949) 271.
 21. R. BULLOUGH and J. J. GILMAN, *J. Appl. Phys.* **37** (1966) 2283.
 22. J. H. O. VARLEY, *Nature* **174** (1954) 886.
 23. *Idem*, *J. Nucl. Energy* **1** (1954) 130.
 24. J. O. STIEGLER and T. S. NAGGLE, *J. Appl. Phys.* **33** (1962) 1894.
 25. P. K. HAFF, *Appl. Phys. Letters* **29** (1976) 473.
 26. R. KATZ and E. J. KOBETICH, *Phys. Rev.* **170** (1968) 401.
 27. R. KATZ, *Nuclear Track Detection* **2** (1978) 1.
 28. H. A. KHAN, *Nucl. Instr. Meth.* **128** (1975) 245.
 29. H. A. KHAN and I. AHMED, *Radiation Effects* **30** (1976) 159.
 30. S. A. DURRANI, H. A. KHAN, R. K. BULL, G. W. DARLING and J. H. FREMLIN, *Geochim-cosmochim Acta* **5** (3) (1974) 254.
 31. K. THIEL, H. KULZER and W. HERR, *Nuclear Track Detection* **2** (1978) 127.
 32. J. A. BRINKMAN, *Amer. J. Phys.* **24** (1955) 246.
 33. A. COLEBROOK and A. H. WINDLE, "Scanning Electron Microscopy: Systems and Applications" (Institute of Physics, London, 1973) p. 132.
 34. M. MONNIN, *Radiation Effects* **5** (1970) 69.
 35. J. FAIN, M. MONNIN and M. MONTRET, Proceedings of the 3rd Symposium on Radiation Chemistry, Tihany, Hungary (1971).
 36. H. A. KHAN, M. A. ATTA, S. YAMEEN, M. R. HAROOM and R. HUSAIN, *Nucl. Instr. Meth.* **127** (1975) 105.
 37. A. N. GOLAND and E. D. MATEOSIAN, *ibid* **106** (1973) 295.
 38. A. MOZUMDER, Charged Particle Tracks and their Structure, in "Advances in Radiation Chemistry", Vol. 1, edited by M. Burton and J. L. Magle (Interscience, New York, 1970).
 39. A. A. MILLER, E. J. LAWTON and J. S. BAFWIT, *J. Polymer Sci.* **14** (1959) 503.
 40. K. BECKER, "Topics in Radiation Dosimetry, Radiation Dosimetry Supplement 1", edited by F. H. Attix (Academic Press, New York and London, 1972) Ch. 2.
 41. *Idem*, "Solid State Dosimetry" (CRC Press, Cleveland, Ohio, 1973) Ch. 5.
 42. F. A. BOVEY, "The Effects of Ionizing Radiation on Natural and Synthetic High Polymers" (Interscience, New York, 1958).
 43. A. CHARLESBY, "Atomic Radiation and Polymers" (Peraon, Oxford, 1969).
 44. A. CHAPIRO, "Radiation Chemistry of Polymeric Systems" (Interscience, New York, 1962).
 45. M. DOLE (Ed.), "The Radiation Chemistry of Macromolecules", Vols. 1 and 2 (Academic Press, New York, 1973).
 46. K. R. SPURNY and J. P. LODGE JUN, NCAR Technical Note STR 77, Vol. 1; Techniques and Discussion, Vol. 2 (1972) Table 3.
 47. J. ANNO, D. BLANC and J. L. TEYSSIER, Proceedings of the Seventh International Colloquium on Corpuscular Photography and Visual Solid Detectors, Barcelona (1970) p. 543.
 48. P. B. PRICE and R. L. FLEISCHER, *Ann. Rev. Nucl. Sci.* **21** (1971) 295.
 49. H. A. KHAN and S. A. DURRANI, *Nucl. Instr. Meth.* **98** (1972) 229.
 50. A. ALI and S. A. DURRANI, *Nuclear Track Detection* **1** (1977) 107.
 51. R. L. FLEISCHER, P. B. PRICE and R. T. WOODS, *Phys. Rev.* **88** (1969) 563.
 52. W. G. JOHNSON, *Prog. Ceram. Sci.* **2** (1961) 1.
 53. M. MONNIN, H. BESSON, S. SANGELLE and A. ARAN, *Comp. Rend., Acad. Sci. Paris* **B264** (1967) 1751.
 54. W. ENGE, K. GRABISCH, R. BEAUJEAN and K. P. BATHOLMA, *Nucl. Instr. Meth.* **115** (1974) 263.
 55. H. A. KHAN and S. A. DURRANI, *Radiation Effects* **13** (1972) 257.
 56. C. E. BLANFORD JUN., R. M. WALKER and J. P. WEFEL, *ibid* **3** (1970) 263.
 57. W. ENGE, K. GRABISCH, L. DALLMEYER, K. -P. BARTHOLOMA and R. BEAUJEAN, *Nucl. Instr. Meth.* **127** (1975) 125.
 58. J. DUTTRANNOIS, Proceedings of the International Congress, Protection Against Accelerator and Space Radiation, CERN-71-16, Vol. 1 (CERN, Geneva, 1971) p. 27/1.
 59. H. B. LÜCK, *Nucl. Instr. Meth.* **131** (1975) 105.
 60. K. ENDO and T. DOKE, *ibid* **111** (1973) 29.
 61. T. A. GRUHN, E. V. BENTON and C. H. ANDRUS, *ibid* **119** (1974) 131.
 62. H. G. PARETZKE, T. A. GRUHN and E. V. BENTON, *ibid* **107** (1973) 597.
 63. G. SOMOGYI, M. VARNAGY and L. MEDVECZKY, *Radiation Effects* **5** (1970) 111.
 64. B. SCHLENK, B. SOMOGYI and A. VALEK, *ibid* **24** (1975) 247.
 65. F. A. COTTON and G. WILKINSON, "Advanced Inorganic Chemistry", 3rd edn (Interscience, Wiley, New York, 1972).
 66. W. T. CRAWFORD, W. DESORBO and J. S. HUMPHREY, *Nature* **220** (1968) 1313.
 67. G. SIEGMON, K. P. BARTHOLOMA and W. ENGE, *Nucl. Instr. Meth.* **128** (1975) 461.

68. G. SOMOGYI, *Radiation Effects* **16** (1972) 233.
69. R. HENKE, E. V. BENTON and H. H. HECKMANN, *ibid* **3** (1970) 43.
70. W. DESORBO and J. S. HUMPHREY, *ibid* **3** (1970) 281.
71. K. BECKER, *Rad. Res.* **36** (1968) 107.
72. W. W. SCHULTZ, *J. Appl. Phys.* **44** (1970) 510.
73. L. J. PILIONE, *Radiation Effects* **33** (1977) 35.
74. A. J. W. GLEADOW and J. F. LOVERING, *Earth Planet Sci. Letters* **22** (2) (1974) 163.
75. T. A. GRUHN, E. V. BENTON and C. H. ANDRUS, *Nucl. Instr. Meth.* **119** (1974) 125.
76. R. K. BULL and S. A. DURRANI, *Geochim. Cosmochim. Acta Suppl.* **6** Proceedings of the 6th Lunar Science Conference, Vol. 3 (1975) 3527.
77. M. S. MANTOVANI, *Earth Plan.* **24** (1974) 311.
78. R. L. FLEISCHER and P. B. PRICE, *Science* **140** (1963) 1221.
79. P. B. PRICE, D. LAL, A. S. TAMHANE and V. P. PERELYGIN, *Earth Planet Sci. Letters* **19** (1973) 377.
80. P. F. GREEN and S. A. DURRANI, *Nuclear Track Detection* **1** (1977) 33.
81. A. AFRAMIAN, *Radiation Effects* **33** (1977) 95.
82. J. A. MORLEY, *Amer. Nucl. Soc. Trans.* **15** (1972) 120.
83. L. MEDVECZKY, Proceedings of the International Conference on Nuclear Track Registration in Insulating Solids, Clermont-Ferrand, Section III, pp. 2–13.
84. Kodak-Pathe, Instructions for the Use of CA80-15 Film and LR115 Film, type I and type II.
85. M. VARNAGY, I. SZABO, S. JUHASZ and I. CSIKAI, *Nucl. Instr. Meth.* **106** (1973) 301.
86. G. P. DIXON and J. G. WILLIAMS, *ibid* **135** (1976) 293.
87. M. G. SEITZ, R. M. WALKER and B. S. CARPENTER, *J. Appl. Phys.* **44** (1973) 510.
88. H. F. SHERWOOD, U.S. Patent 3 501 636 (1970).
89. F. GEISLER and P. R. PHILLIPS, *Rev. Sci. Instrum.* **43** (1972) 283.
90. D. R. STONE, *Health Phys.* **16** (1969) 772.
91. H. B. LUCK, *Nuclear Track Detection* **2** (1978) 147.
92. J. BLOK, J. S. HUMPHREY and J. E. NICHOLS, *Rev. Sci. Instrum.* **40** (1969) 509.
93. R. L. FLEISCHER, P. B. PRICE and R. M. WALKER, *ibid* **37** (1966) 525.
94. J. W. N. TUYN, *Nucl. Appl.* **3** (1967) 372.
95. A. I. KHOVANIVICH, G. L. PIKALOV and I. F. KRYVOKRYSENKO, *At. Energy* **29** (1970) 367.
96. H. A. KHAN, *Radiation Effects* **8** (1971) 135.
97. M. VARNAGY, J. SZABO, S. JUHASZ and J. CZIKAI, *Nucl. Instr. Meth.* **106** (1973) 301.
98. M. M. MONNIN and G. E. BLANFORD, *Science* **181** (1973) 743.
99. P. J. OUSEPH, *Phys. Rev. Letters* **30** (1973) 1162.
100. B. DÖRSCHEL, *Kernenergie* **12** (1969) 303.
101. H. A. KHAN and S. A. DURRANI, *Nucl. Instr. Meth.* **101** (1972) 583.
102. K. BECKER, *Health Phys.* **12** (1966) 955.
103. V. I. PRIBYTOV and B. S. ROZOV, *Instr. Exp. Tech.* **18** (4) Part I, January (1976) 1007.
104. D. JOWITT, *Nucl. Instr. Meth.* **92** (1971) 37.
105. C. B. BESANT and E. R. TRUCK, *The Microscope* **20** (1) (1972) 127.
106. T. LYCOS and C. B. BESSANT, *ibid* **24** (3) (1976) 199.
107. E. POLIG, *Int. J. Appl. Radiat. Isot.* **26** (9) (1975) 519.
108. A. A. HARMS and M. S. MONIZ, *Nucl. Instr. Meth.* **121** (1974) 477.
109. W. G. CROSS and L. TOMMASINO, *Radiation Effects* **5** (1970) 85.
110. F. J. CONGEL and J. N. ROBERTS, *Nucl. Instr. Meth.* **100** (1972) 147.
111. G. SOMAGYI and J. GULIAS, *Radiosotropy* **13** (1972) 5, 49.
112. W. G. CROSS and L. TOMMASINO, Proceedings of the Symposium on Neutron Dosimetry in Biology and Medicine, Neuherberg, Germany (1972).
113. M. VARNAGY, E. GYARMATIC and T. SZTARISKA, *Nucl. Instr. Meth.* **133** (1976) 371.
114. K. BECKES and M. ABD-EL-RAZEK, *ibid* **124** (1975) 557.
115. E. JASIAK and E. PIESCH, *ibid* **128** (1975) 447.
116. A. M. BHAGURAT, H. SINGH and S. D. SOMAN, *ibid* **138** (1976) 173.
117. M. VARNAGY, E. GYARMATI and T. SZTARISKA, *ibid* **113** (1976) 371.
118. D. L. WINTER, K. SURI, J. A. D'URSO, F. L. COTA, W. W. ASHLEY, R. M. BINNARD, W. HAYMAKER, E. V. BENTON, M. R. CRUTY and W. ZEMAN, *Aviat. Space Environ. Med.* **45** (1975) 494.
119. R. M. WALKER, P. B. PRICE and R. L. FLEISCHER, *Appl. Phys. Letters* **3** (1963) 28.
120. A. L. FRANK and E. V. BENTON, *Nuclear Track Detection* **1** (1977) 149.
121. J. E. GINGRICH and D. B. LOVETT, *Trans. Amer. Nucl. Soc.* **15** (1972) 118.
122. J. E. GINGRICH, *Power Eng.* August (1973) 48.
123. Y. QUERE, J. C. RESNEAU and J. MORY, *Compt. Rend. Acad. Sci. Paris* **262** (166) 1528.
124. Y. QUERE and H. COUVE, *J. Appl. Phys.* **39** (1968) 4012.
125. J. MORY and G. DELSARTE, *Radiation Effects* **1** (1969) 1.
126. J. MORY, D. DE GUILLEBON and G. DELSARTE, *ibid* **5** (1970) 37.
127. M. VOBECKY and E. LEDROVA, *Radiochem. Radioanal. Letters* **24** (1976) No. 3, 199.
128. J. R. WEISS and E. L. HAINES, *Rev. Sci. Instrum.* **45** (1974) 606.
129. B. GRAVERT, M. G. SEITZ and G. SAPTRAJANDRA, *Earth Planet Sci. Letters* **21** (1974) 389.
130. G. M. REIMER, *Radiochem. Radioanal. Letters.* **21** (1975) 339.
131. M. WALD and G. WIEGARD, *Radiochem. Acta* **19** (1973) 37.
132. J. L. BOUTAINE and A. LEMONNIER, *Mem. Sci. Res. Met.* **70** (1973) 747.
133. R. BEAUJEAN and W. ENGE, *Nuclear Track Detection* **1** (1977) 19.
134. P. B. PRICE, R. L. FLEISCHER, P. D. PETERSON, C. O'CEALLAIGH, P. O'SULLIVAN and A.

- THOMPSON, *Phys. Rev.* **164** (1967) 1618.
135. R. P. HENKE and E. W. BENTON, *Nuclear Track Detection I* (1977) 93.
136. P. F. GREEN and S. A. DURRANI, *ibid* **1** (1977) 33.
137. R. A. STERN and P. B. PRICE, *Nature Phys. Sci.* **240** (1972) 82.
138. R. L. FLEISCHER, H. R. HART and W. R. GIARD, *Science* **170** (1970) 1189.
139. Nuclepore Corporation, 7035 Commerce Circle, Pleasanton, California.
140. M. C. PORTER and H. J. SCHNEIDER, *Filtration Eng.* January/February (1973) 8.
141. C. P. BEAN, M. V. DOYLE and G. ENTINE, *J. Appl. Phys.* **41** (1970) 1454.
142. C. P. BEAN, "Membranes - A Series of Advances", edited by G. Eisenman, Vol. 1 (Dekker, New York, 1972) p. 1.
143. R. FRANK, K. R. SPURNY, D. C. SHEESLEY and J. P. LODGE Jr, *J. Microscopie* **9** (1970) 735.
144. J. STANIM, *Tappi* **54** (1971) 1909.
145. R. L. FLEISCHER, J. R. M. VIERTL and P. B. PRICE, *Rev. Sci. Instrum.* **43** (1972) 1708.
146. J. SONG, P. FROM, W. MORRISSEY and J. SAMS, *Cancer* **28** (1971) 553.
147. P. T. WERTAKE, B. A. MARKOVETS and S. STELLAR, *Acta. Cytologica* **16** (1972) 224.
148. J. R. RICH, *Bull. Los Angeles Neurological Soc.* **34** (1969) 115.
149. E. B. KING and W. M. RUSSELL, *Acta Cytologica* **11** (1967) 319.
150. General Electric-International **7** (3) (1971) 3-5.
151. K. R. SPURNY, J. P. LODGE Jr, E. R. FRANK and D. C. SHEESLEY, *Environmental Sci. Technol.* **3** (1969) 464.
152. K. R. SPURNY and J. P. LODGE Jr, *Aerosol Sci.* **3** (1972) 407.
153. S. TWOMEY, *J. Atmos. Sci.* **29** (1972) 318.
154. D. A. HORWITZ and M. A. GARRETT, *J. Immunology* **103** (1971) 649.
155. R. W. DE BLOIS and C. P. BEAN, General Electric Company preprint (1973) 73-CRD-188.
156. W. H. COULTER, U.S. Patent 2 656 509. Coulter Bulletin (T1). The Theory of the Coulter Counter. Coulter Electronics Ltd., Cold Harbour, Herts. AL5 4UN, UK.

Received 22 March and accepted 11 July 1979.